

Jiří Čtyroký; Rolf Göring; Jiří Janta; Wolfgang Karthe; Andreas Rasch; Mathias Rottschalk; Josef Schröfel

Integrated electrooptic modulators and switches in  $LiNbO_3$

*Kybernetika*, Vol. 26 (1990), No. 3, 171--190

Persistent URL: <http://dml.cz/dmlcz/125575>

## Terms of use:

© Institute of Information Theory and Automation AS CR, 1990

Institute of Mathematics of the Academy of Sciences of the Czech Republic provides access to digitized documents strictly for personal use. Each copy of any part of this document must contain these

*Terms of use.*



This paper has been digitized, optimized for electronic delivery and stamped with digital signature within the project *DML-CZ: The Czech Digital Mathematics Library*  
<http://project.dml.cz>

## INTEGRATED ELECTROOPTIC MODULATORS AND SWITCHES IN $\text{LiNbO}_3$

JIŘÍ ČTYROKÝ, ROLF GÖRING, JIŘÍ JANTA, WOLFGANG KARTHE,  
ANDREAS RASCH, MATHIAS ROTTSCHALK, JOSEF SCHRÖFEL

The principles of electrooptic guided wave modulators and switches are described briefly, namely of the phase modulator, Mach-Zehnder interferometric modulator, directional coupler modulator/switch and different types of an X-switch. The titanium indiffusion as the most widely used method for fabricating the integrated-optical components is compared with the proton exchange technology. The stability problems, e.g. optical damage, thermal and electrical drift phenomena, and the methods of overcoming them are mentioned, too. Experimental results achieved in the authors' laboratories with Mach-Zehnder modulators, directional coupler switch and X-switches are presented.

### CONTENTS

1. Introduction 172
2. Principles of operation 172
  - 2.1 Phase modulation 173
  - 2.2 Mach-Zehnder interferometric modulator 174
  - 2.3 Directional-coupler switch 175
  - 2.4 X-switch (BOA) 177
  - 2.5 Polarization-independent and travelling-wave switches 179
3. Fabrication technology 180
  - 3.1 Titanium diffusion 180
  - 3.2 Proton exchange 181
  - 3.3 Electrode and device fabrication 182
4. Stability problems 182
  - 4.1 Photorefractive effect ("optical damage") 182
  - 4.2 Pyroelectric effects 183
  - 4.3 DC drift phenomena 184
5. Experimental results 184
  - 5.1 Mach-Zehnder interferometric modulators 184
  - 5.2 Directional-coupler switch 185
  - 5.3 X-switches 186
6. Conclusions 187
  - References 188

## 1. INTRODUCTION

Nearly two decades ago, a new concept of creating guided-wave optical "integrated circuits" which consist of several optical components on a common substrate was suggested [1]. Nowadays, the first commercial integrated-optical devices are becoming available. The most mature technology for fabricating integrated-optical components and circuits is the diffusion of titanium into a single crystal of lithium niobate [2]. However, other methods like proton exchange in  $\text{LiNbO}_3$  [3] are used, too. High-quality low-loss single-mode (or few-mode) planar and channel optical waveguides can be fabricated with acceptable reproducibility. Very good electrooptic, piezoelectric, acoustooptic as well as optical nonlinear properties of lithium niobate may be fully utilized in guided-wave optical devices.

In this contribution we briefly describe the principles of operation of the particular class of electrooptic guided wave modulators and switches, namely, the phase modulator, Mach-Zehnder interferometric modulator [4], directional coupler switch [5], [6] and the X-switch [7] or the so called BOA switch [8]. These components form the most important building blocks for more complicated devices with higher level of integration [9–13]. Two fabrication processes using  $\text{LiNbO}_3$  substrates, namely the titanium diffusion and the proton exchange, are described. The problems which affect the stability of the  $\text{LiNbO}_3$  devices, i.e. the photorefractive effect and voltage drifts, are discussed, too. Finally, some recent experimental results obtained in the authors' laboratories are presented.

## 2. PRINCIPLES OF OPERATION

Single-mode waveguides are created in  $\text{LiNbO}_3$  by selectively increasing the refractive index near the crystal surface, e.g. by the diffusion of titanium [2] or by proton exchange [3]. The application of an external electric field  $\mathbf{E}$  affects the permittivity tensor  $\boldsymbol{\varepsilon}$  of the crystal by

$$\Delta(\boldsymbol{\varepsilon}^{-1}) = \mathbf{r} \cdot \mathbf{E}, \quad (1)$$

or, in Cartesian coordinates,

$$\Delta\varepsilon_{jr} = -\varepsilon_{jl}r_{lr}q_{pr}^2, \quad (2)$$

where  $\mathbf{r}$  is the electrooptic tensor.

Most electrooptic guided-wave devices make use of the strongest electrooptic coefficient  $r_{333}$  (or, in the usual shortened notation,  $r_{33}$ ). In this case, both the major component of the electric field intensity of the guided mode and the external applied electric field have to be parallel with the optic axis ( $Z$  or  $c$  axis) of the  $\text{LiNbO}_3$  crystal. The refractive index change due to the electrooptic effect is then

$$\Delta n = \Delta(\varepsilon_{33}^{1/2}) = -\frac{1}{2}n^3r_{33}E_3. \quad (3)$$

## 2.1 Phase modulation

A guided mode of the waveguide is characterized by its propagation constant  $\beta$ , or the effective refractive index  $N = \beta/k$ ,  $k = 2\pi/\lambda$  being the wavenumber and  $\lambda$  the free-space wavelength. The external field change the effective index  $N$  via the electrooptic effect by

$$\Delta N = \iint_{-\infty}^{\infty} \Delta n e^2(x, y) dx dy = -\frac{1}{2}n^3r_{33} \iint_{-\infty}^{\infty} E_3 e^2(x, y) dx dy, \quad (4)$$

where  $e(x, y)$  is the normalized transversal distribution of the mode field amplitude. Applying the external electric field over the length  $L$  of a channel waveguide, the phase of the optical wave is changed by

$$\Delta\phi = kL\Delta N. \quad (5)$$

Two typical arrangements of the guided-wave phase modulators are shown in Fig. 1.

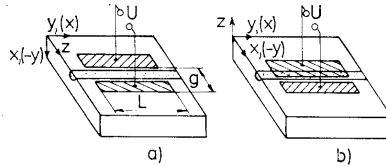


**Fig. 1.** a) *X*-cut *Y*-propagating (or *Y*-cut *X*-propagating) phase modulator, b) *Z*-cut *Y*- or *X*-propagating phase modulator.

The waveguide in Fig. 1a is fabricated in an *X*-cut or *Y*-cut crystal. The guided wave of TE polarization (its electric field is parallel to the waveguide surface) is affected by the horizontal component of the electric field created by two symmetric electrodes. In the *Z*-cut crystal (Fig. 1b), the operating polarization of the guided wave is TM (its electric field roughly perpendicular to the waveguide surface), and the vertical component of the applied electric field is used. The electrodes are therefore asymmetric with respect to the waveguide.

The important parameter of the phase modulator is the half-wave voltage  $U_\pi$  needed to reach the phase shift  $\Delta\phi = \pi$ . Since  $U_\pi$  is inversely proportional to the electrode length  $L$ , the voltage-length product  $U_\pi L$  is the suitable measure of the “effectivity” of modulation. From (4) and (5) it follows

$$U_\pi L = \frac{\lambda g}{n^3 r_{33} F}, \quad (6)$$

where  $g$  is the gap between the electrodes, and

$$F = \iint_{-\infty}^{\infty} \frac{E_3 d}{U} e^2(xy) dx dy \quad (7)$$

is the overlap integral of the optical and the applied electric fields. Taking the realistic

values of  $r_{33} = 30 \times 10^{-12} \text{ m/V}$ ,  $g = 3 \mu\text{m}$ ,  $F \approx 0.3$ ,  $\lambda = 1 \mu\text{m}$  and  $n = 2.2$ , we obtain the value of  $U_{\pi}L = 30 \text{ V mm}$ .

For high applied voltages of several tens of volts applied across a gap of several micrometers, the above simple description is inadequate. The electrooptic index change becomes comparable with the magnitude of the refractive index variations creating the waveguide and may affect the guiding properties, so that nonlinearity in phase modulation and even parasitic amplitude modulation (the “cut-off” modulation) can take place.

Phase modulators are important components of high-speed coherent optical transmission systems [10] and optical fibre sensors [14]. Phase modulation may easily be converted into intensity modulation and switching. Although other methods of intensity modulation and switching have been proposed, too, the devices based on the phase modulation exhibit considerably lower switching voltages and/or better performance.

## 2.2 Mach-Zehnder interferometric modulator

Perhaps the simplest but the most efficient amplitude modulator is the Mach-Zehnder interferometric modulator [4] shown in Fig. 2a.

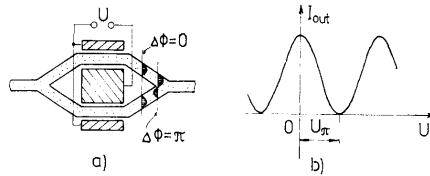


**Fig. 2.** a) Arrangement of X-cut Mach-Zehnder interferometric modulator. The field distributions in the output branching for the phase shift  $\phi = 0$  and  $\phi = \pi$  is shown, b) The modulation characteristics of the modulator.  $U_{\pi}$  is the half-wave (modulation) voltage.

Light fed into the (single-mode) input waveguide is symmetrically divided into two arms in which mutually opposite electrooptic phase changes take place. The output branching combines light from both arms into the single-mode output waveguide. If the phase shift between the arms is equal to zero (or an even multiple of  $\pi$ ), the optical field distribution in the output branching is symmetric, as shown in Fig. 2a for  $\Delta\phi = 0$ , and the (fundamental) mode is excited in the output waveguide. If the phase shift differs by an odd multiple of  $\pi$ , the optical field distribution in the output branching is antisymmetric (see Fig. 2a for  $\Delta\phi = \pi$ ). The only (fundamental) mode of the output waveguide thus cannot be excited, and light is radiated into the substrate out of the waveguide.

The modulation characteristics of the interferometric modulator is sinusoidal, as shown in Fig. 2b:

$$I_{\text{out}} = \frac{1}{2}I_{\text{in}}[1 + \cos(\pi U/U_{\pi} + \phi)]. \quad (8)$$

Due to the “push-pull” effect in both arms, the voltage-length product is just one half of that of a phase modulator (6),

$$U_{\pi}L = \frac{\lambda g}{2n^3 r_{33} F}, \quad (9)$$

where the factor  $F$  is given by (7).

The phase shift  $\phi$  in (8) accounts for possible asymmetry of the modulator arms due to fabrication imperfections.

An important parameter of the real modulator is the extinction ratio

$$c_E = 10 \log \frac{I_{\min}}{I_{\max}} \text{ [dB]}, \quad (10)$$

where  $I_{\min}$  and  $I_{\max}$  are the minimum and maximum output light intensities, respectively. In well-made modulators, this value is below  $-20$  dB.

### 2.3 Directional-coupler switch

Directional coupler is formed by two parallel identical waveguides in proximity so that light in one of them is coupled to the other via evanescent fields. Although for rigorous analysis of its switching properties the concept of symmetrical and antisymmetrical modes is used [15], it is more illustrative to explain its operation on the basis of coupled waves. The coupling depends upon the waveguide parameters, interwaveguide separation and wavelength. For an appropriate length of coupling section, called the coupling length  $L_c$ , all the light entering one waveguide passes over into the other. In general, if the difference  $\Delta\beta = \beta_1 - \beta_2$  of propagation constants is induced by electrooptical effect, the light power coupled into the second waveguide along the length  $L$  is [16]

$$\frac{I_2(L)}{I_1(0)} = \frac{1}{1 + \left(\frac{\Delta\beta L_c}{\pi}\right)^2} \sin^2 \left\{ \frac{\pi L}{2L_c} \left[ 1 + \left(\frac{\Delta\beta L_c}{\pi}\right)^2 \right]^{1/2} \right\}. \quad (11)$$

Obviously, the total light transition (cross state  $\otimes$ ) is possible only for  $\Delta\beta = 0$  and  $L = L_c, 3L_c, \dots$ . On the contrary, if we set, e.g.,  $\Delta\beta = (\pi/L_c)\sqrt{3}$ ,  $L = L_c$ , all the light comes back into the first waveguide (bar state  $\ominus$ ). In this way the switching (or modulation) function is accomplished. In Fig. 3a the corresponding arrangement is shown schematically for the case of a coupler on  $z$ -cut  $\text{LiNbO}_3$  substrate. Uniform electrodes cover the entire coupling section. Figure 3b presents the distribution of the light along the coupling section for both cross and bar states. The diagram in Fig. 3c illustrates the critical working conditions of this type of coupler: whilst the bar state can be realized along the arcs depicted, the cross state occurs only in isolated points on the vertical axis. Thus, there is no possibility to adjust the cross state electro-optically and, consequently, the influence of fabrication tolerances on the cross-state crosstalk cannot be compensated.

To achieve the possibility of adjusting electrically both states of the switch the technique of  $\Delta\beta$  reversal is used. The simplest arrangement of this type is shown schematically in Fig. 3d: the electrodes are split into two equal parts driven with opposite

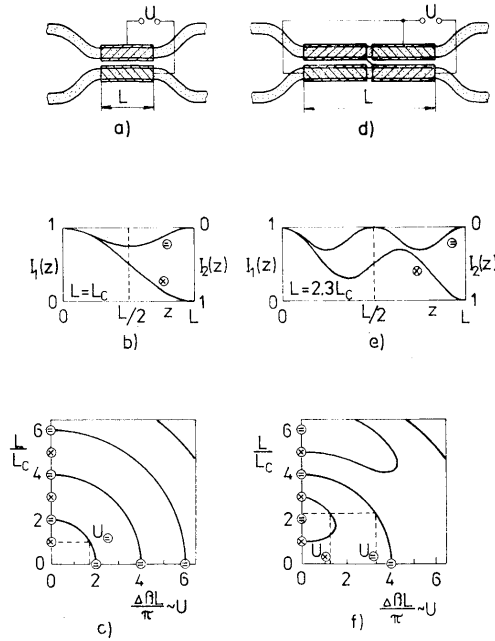


**Fig. 3.** Schematic lay-out of uniform (a) and  $\Delta\beta$ -reversal (b) directional coupler, corresponding distributions of the light along the coupling sections (b, e) and switching diagrams (c, f).

polarity voltages. The switching diagram in Fig. 3f shows that the cross state can be adjusted by  $\Delta\beta$ , i.e. by the voltage, for the length  $L$  from the interval  $\langle L_c, 3L_c \rangle$ . As a result, the switching is obtained by changing the voltage  $U_e$  from  $U_\ominus$  to  $U_\otimes$ : the minimum switching voltage  $\Delta U_e = U_\otimes - U_\ominus$  is obtained for  $L \approx 2.3L_c$ .

In Fig. 4 the switching (modulation) characteristics are presented for both uniform

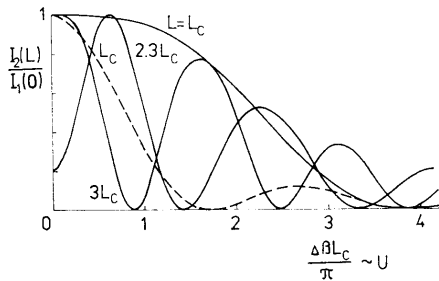


**Fig. 4.** Switching characteristics of uniform (dashed line) and  $\Delta\beta$ -reversal (solid lines) directional couplers. All curves are symmetrical against the vertical coordinate axis.

and  $\Delta\beta$ -reversal switch, in the latter case for limiting lengths  $L = L_c, 3L_c$  and for optimum length  $L \approx 2.3L_c$ . It can be seen that the optimum  $\Delta\beta$ -reversal arrangement results in much less switching voltage if compared with the uniform variant, naturally at the expense of the overall length of the switch.

Nevertheless, the voltage-length product of the optimum  $\Delta\beta$ -reversal arrangement is close to that of a uniform variant,  $L = L_c$ . It has been found [17] that the voltage-length product is in this case

$$U_\pi L = \frac{\sqrt{3}}{2} \frac{\lambda g}{n^3 r_{33} F}, \quad (12)$$

where

$$F = \iint_{-\infty}^{\infty} \frac{E_3 g}{U} e_s e_a dx dy; \quad (13)$$

here  $e_s$  and  $e_a$  are the field distributions of the symmetric and antisymmetric modes of the whole double-guide structure in the coupling region, respectively. For weak coupling, (13) approaches (7).

An important parameter of the switch is the crosstalk

$$c_T = -10 \log \frac{I_{\text{off}}}{I_1 + I_2} [\text{dB}], \quad (14)$$

where  $I_{\text{off}}$  is the light intensity in the switched-off output, and  $I_1 + I_2$  is the sum of light intensities in both outputs.

It has been shown recently [18] that the coupling between the waveguides in the separating region outside the electrodes prevents the perfect switching and thus affects the attainable crosstalk. To avoid this, the electrodes should be extended to the separating regions.

Typical experimental crosstalk levels of the directional-coupler switch lie well below  $-20$  dB; values lower than  $-30$  dB have been reported, too.

## 2.4 X-switch (BOA)

The simplest electrooptic switch is probably the X-switch [7] shown in Fig. 5a,b. The basic principle of its operation has been found to be identical with the BOA switch (Fig. 5c) designed earlier [8].

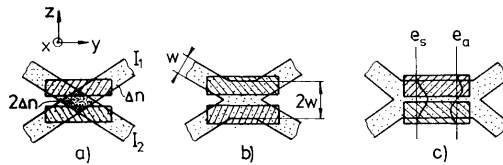


**Fig. 5.** Three configurations of X-type switches on X-cut Y-propagating  $\text{LiNbO}_3$  substrate: a)  $2\Delta n$  X-switch, b)  $2w$  X-switch, c) BOA switch with the field distributions (common also for a and b) of the symmetric ( $e_s$ ) and antisymmetric ( $e_a$ ) modes in the central region.

Roughly speaking, the waveguide structure of the BOA switch is nothing but the directional coupler with a zero gap between the waveguides in the “coupling region”; the waveguide in the central part of the BOA switch should support two guided modes. The X-switch in Fig. 5a,b is the “shortened version” of the BOA switch. To ensure the propagation of two modes in the central region, the index change in Fig. 5a or the waveguide width in Fig. 5b are correspondingly increased. Light coupled into one input arm excites both modes – symmetric and antisymmetric ones – with equal amplitudes.

The field distribution of both modes is shown in Fig. 5c. The horizontal electric field component  $E_3$  induced by the electrodes affects the symmetric mode more strongly than the antisymmetric one. In this way, the applied voltage changes the

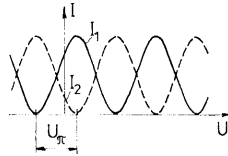


Fig. 6. The ideal switching characteristics of the X-type switch.

mutual phase shift between the two modes, and, correspondingly, the light distribution between the output waveguides. The switching characteristic is, in general, periodic, as shown in Fig. 6. The voltage-length product can easily be found to be [17]

$$U_{\pi}L = \frac{\lambda g}{n^3 r_{33} F} \quad (15)$$

with

$$F = \iint_{-\infty}^{\infty} \frac{E_3 g}{U} (e_s^2 - e_a^2) dx dy. \quad (16)$$

It has been shown that the switching voltage of this type of switch is comparable or even less than that of a directional coupler of comparable length [17]. The advantage of the X-switch of Figs. 5a,b consists in its simple geometry and easy integrability into larger switching matrices without the need of waveguide bends [12]. However, the overall length of the switch is very short (typically, about 1 mm) so that the switching voltage of several tens volts is needed. In this case, large electrooptic changes of the refractive index modify the switching characteristics so that they deviate from strictly periodic behaviour.

The crosstalk of the X-type switches is, in fact, determined by the actual switch symmetry and cannot be electrooptically fine-tuned like in the directional coupler. The analyses [19, 20] show that only small deviations of the waveguide widths or index changes from symmetry (by 2–3%) are allowed in the branching regions to keep the crosstalk below a reasonable level of –20 dB. Interesting relations between the switch symmetry and the switching characteristics have been found [19].

## 2.5 Polarization-independent and travelling-wave switches

Two important features of guided-wave optical devices have not been discussed yet. It is the dependence of the device characteristics on the polarization of the input light, and, on the other hand, the speed, or the frequency limit, of the modulation and switching.

The inherent polarization dependence of the electrooptic devices is the direct consequence of the direction-dependent (tensorial) character of the electrooptic effect. Moreover, even the waveguiding properties of  $\text{LiNbO}_3$  devices depend on the polarization due to the anisotropy of the crystal properties. In general, to each polarization-independent operation of the device, two conditions are to be fulfilled: to reach similar waveguiding properties (at least the mode field distribution) for both (quasi-) TE and TM polarizations by suitable fabrication conditions, and to ensure the electrooptic control of both polarizations via suitable electrode configuration. Usually, the electrooptic coefficient  $r_{33}$  is used to control the extraordinary polarization, and about three-times smaller coefficient  $r_{13}$  to control the ordinary one. In both cases, the same  $E_3$  component of the applied electric field is utilized, which prevents independent control of both polarizations. Nevertheless, the polarization independent operation of guided-wave optical devices has been successfully demonstrated. One of the examples is the polarization-independent directional coupler switch with two sections of  $\Delta\beta$ -reversal and simultaneous coupling tuning [21].

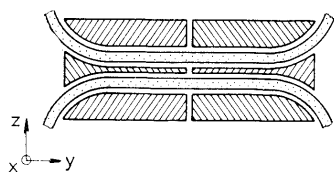


**Fig. 7.** Polarization-independent directional coupler switch utilizing  $\Delta\beta$  reversal and coupling tuning on the X-cut  $\text{LiNbO}_3$ .

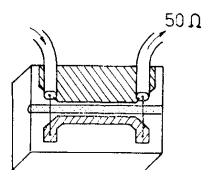


**Fig. 8.** Travelling-wave phase modulator with asymmetric coplanar electrodes.

The arrangement is shown in Fig. 7. To reach low crosstalk in both states, the technique of weighted coupling [22] is used. Similarly to all polarization-independent switches, the switching voltage is several times (5 to 9-times) higher than for the single-polarization devices.

The speed of standard lumped-electrode modulators or switches is limited by the RC constant of the electrode capacitance and the matched load, usually  $50\ \Omega$ . The typical electrode capacitance is of the order of several picofarads which leads to the modulation bandwidth of several GHz. To overcome the bandwidth limitation by RC constant, the travelling-wave electrodes in the form of a short piece of an impedance-matched transmission line are used [23]. The asymmetric coplanar electrode arrangement as shown in Fig. 8 is preferred since it is easier to be matched

to the standard  $50\ \Omega$  coaxial feeder than the symmetric coplanar electrodes. However, other configurations have been successfully used, too [24].

The basic physical phenomenon limiting the modulation bandwidth of a travelling-wave device is the velocity mismatch between the optical and modulation (microwave) waves. For uniform electrodes of the length  $L$ , the attainable 3-dB bandwidth is

$$B \approx \frac{0.6C}{L(n_m - n_{opt})} \quad (17)$$

where  $n_m = 4.1$  and  $n_{opt} = 2.15$  are the effective microwave and optical refractive indices, respectively. In standard  $\text{LiNbO}_3$  devices, the  $BL$  product is about  $9\ \text{GHz cm}$ . To increase the modulation bandwidth, methods of velocity mismatch compensation [25] and suppression [26] (at the expense of the modulation efficiency) have been designed and successfully tested resulting in the bandpass and baseband operation, respectively, over several tens of gigahertz.

### 3. FABRICATION TECHNOLOGY

#### 3.1 Titanium indiffusion

The titanium indiffusion (TI) is the most widely-used method for the fabrication of optical waveguides [2]. Successive steps of the technological procedure are presented in Fig. 9a. An optically polished surface of a  $\text{LiNbO}_3$  chip is cleaned and

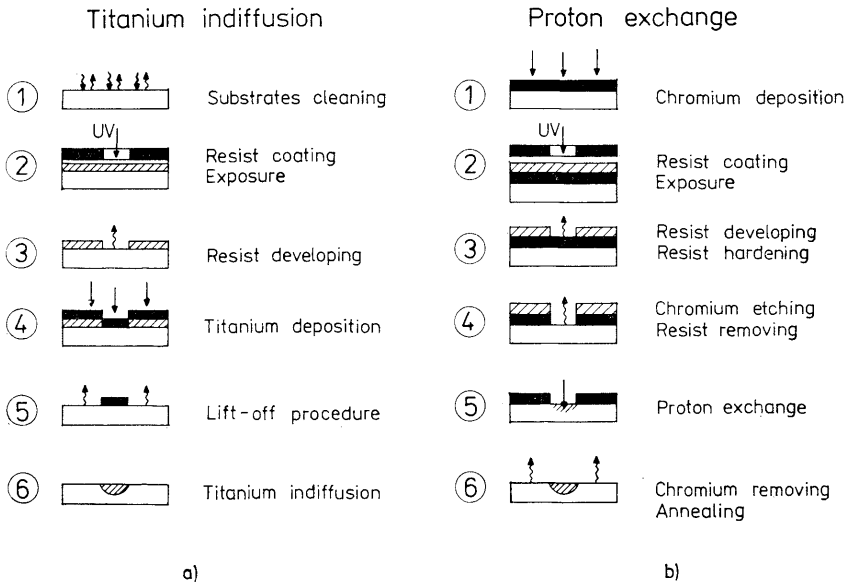


Fig. 9. Two technological procedures for fabricating the waveguiding structures in  $\text{LiNbO}_3$  substrates: a) titanium indiffusion, b) proton exchange.

coated with a uniform resist layer. Using an electron-beam-lithographically produced mask the resist is patterned by lithographic technique. After sputtering or evaporating titanium onto the resist and a subsequent lift-off process the patterned titanium film is indiffused. The Ti layer is 25 to 70 nm thick and the stripe width varies from 3 to 12  $\mu\text{m}$  depending both on the device function and on the optical wavelength. The diffusion takes place under gas atmosphere (argon, oxygen or synthetic air) at 1000 to 1050  $^{\circ}\text{C}$  during diffusion time of 4 to 10 h. The warm-up and cool-down rates are 3–5 K/min. A serious disadvantage of the TI process is the simultaneous out-diffusion of lithium generating parasitic planar waveguide with an increased extraordinary refractive index. In order to suppress this effect a wet atmosphere during indiffusion was proposed [27]. By this method good-quality waveguides can be obtained [28]. Even better results can be obtained by the platinum-box method [29]. The  $\text{LiNbO}_3$  chip is enclosed in a small platinum box and the residual volume of the box is filled with as-grown  $\text{LiNbO}_3$  pieces. The diffusion takes place under an oxygen stream of 0.5 to 1.0 l/min. Inside the box a lithium vapor pressure is generated to suppress the outdiffusion. In that way we fabricated completely out-diffusion-free waveguides for wavelengths down to 476 nm with excellent optical parameters.

The waveguide parameters depend on the titanium thickness and density, the stripe width, the diffusion conditions and the crystal material quality. The diffusion process has to be carried out until the titanium source on the surface is used up completely to prevent the waveguide loss due to rest of the metal. In this case, both ordinary and extraordinary refractive index profiles are of Gaussian form with the 1/e-depth of 2 to 6  $\mu\text{m}$  and  $\Delta n_o$  and  $\Delta n_e$  of the order of  $10^{-3}$  to  $10^{-2}$ .

### 3.2 Proton exchange

The proton exchange (PE) induces changes of the physical properties of the  $\text{LiNbO}_3$  crystal [3]. In this low temperature process ( $T_{\text{PE}} < 350$   $^{\circ}\text{C}$ ), up to 75 percent of lithium ions of the  $\text{LiNbO}_3$  crystal are exchanged by protons (probably in a 1 : 1 proportion). Suitable proton sources are melts of acid inorganic salts and organic acids. Benzoic acid is commonly used with a small content of lithium benzoate acting as an exchange buffer. The proton exchange takes place (see Fig. 9b) through a patterned layer on the  $\text{LiNbO}_3$  surface (suitable materials are Cr, Al, Au or  $\text{Si}_3\text{N}_4$ ). To pattern the layer an etch technology has to be utilized using the same electron-beam-lithographically produced mask as for TI. As a result of PE the extraordinary refractive index is increased (step index profile  $\Delta n_e \approx 0.12$  at  $\lambda = 633$  nm) and the ordinary index is decreased ( $\Delta n_o \approx -0.04$ ). Therefore, only  $n_e$ -active polarized waves can be guided. The most important property of the PE waveguides is their high resistance against optical damage (>4 orders of magnitude in relation to TI-prepared waveguides). On the other hand, they exhibit high loss, temporal instability and a strong decrease of many optical effects, particularly the electrooptic one [30]. In spite of these dis-

advantages the PE is suitable for the fabrication of passive integrated-optic devices such as lenses, grating structures, and acoustooptic elements [31].

Low-loss active integrated-optic devices can be fabricated by an annealing process following the PE [32–34]. The PE waveguide is annealed at temperatures from 300 to 400 °C. In this way low-loss, temporally stable and damage insensitive planar and stripe waveguides can be obtained with a refractive index profile like that of TI-waveguides. The most important fact are the restoration of the electrooptic effect up to the value of the  $\text{LiNbO}_3$  crystal and the damage threshold increase by about one order. However, the electrical conductivity is increased by seven to eight orders of magnitude [33, 34].

### 3.3 Electrode and device fabrication

For high-speed electrooptic devices, the electrodes are made e.g. by deposition of a thin metal layer (e.g. Ni), patterning the layer, again using electron-beam-lithographically produced masks, increasing the electrode pattern thickness by electroplating with gold and etching the thin metal layer outside the electrodes. A simpler method to obtain electrodes for low frequency modulation is the deposition of thinner aluminium electrode pattern

For low loss input/output coupling of the light the high-quality polishing of the substrate edges is required. The edge curvature radius in the waveguide region should be less than 0.1  $\mu\text{m}$  and the waveguide cross-section must be defect-free. The optical fibers are adjusted precisely to the waveguides for maximum overlapping of the light intensity profiles of both light guides. After that the fiber is connected to the waveguide by UV-cured epoxy (the epoxy acts also as an immersion to suppress Fresnel reflection). The fibers must be supported either individually or in V-grooves etched in silicon chips. Minimum coupling loss between fiber and waveguide of 0.15 dB was obtained for precise match of optical light profiles and for well adjusted coupling [49].

## 4. STABILITY PROBLEMS

In a number of papers experimentally observed parameter drifts in  $\text{LiNbO}_3$  waveguide devices have been reported. According to their different origin they can be divided into three groups.

### 4.1 Photorefractive effect (“optical damage”)

When light passes through a  $\text{LiNbO}_3$  crystal, photoionization of  $\text{Fe}^{2+}$  to its  $\text{Fe}^{3+}$  state occurs and the generated free electrons migrate from the illuminated to the dark regions with a current density mainly in the +c direction (photovoltaic effect). The resulting charge separation sets up an internal electric field which locally changes

the refractive index of the illuminated  $\text{LiNbO}_3$  region due to the linear electro-optic effect [35]. The amount of refractive-index change and the time constant of this process depend on the Fe-content of the crystal, the optical intensity and strongly on the wavelength of illumination.

The process mentioned above leads directly to temporal shifts of the output phase of a simple phase modulator. However, till now this effect has not been investigated experimentally in a simple channel waveguide.

For guided-wave Mach-Zehnder interferometers, a considerable drift of the output signal has been observed for strong power imbalance of the two arms at  $\lambda = 0.85 \mu\text{m}$  [36]. For ideal symmetry this kind of drift can be avoided. At  $\lambda = 1.5 \mu\text{m}$  no drift has been observed for optical powers of less than 75 mW [37].

For directional-coupler switches a refractive-index change inside the illuminated channel waveguide leads to changes of the coupling length and can be observed as drift in the switching state. Such a drift has been found to be pronounced at  $0.85 \mu\text{m}$  for a guided-wave power of only  $3.2 \mu\text{W}$  [38]. However, at  $\lambda = 1.3 \mu\text{m}$  no drift could be observed at power levels less than 25 mW [39].

The effect of light-induced scattering must be taken into account, too. It results in a decrease of the waveguide output power with time. Systematic investigations in this field have been performed in the visible region for planar waveguides [40], but for channel waveguides there is a lack of reliable results.

A very complicated situation occurs when light of ordinary polarization is used. In this case the combination of depolarization scattering and off-diagonal elements of the photovoltaic tensor leads to polarization conversion to the extraordinary mode [41]. Additional instabilities appear when an external voltage is applied to the electrode system of a modulator or switch. The photoexcited electrons move under the influence of the applied electric field and tend to compensate it at least partially. The observed drift depends on the photoconductivity in the illuminated waveguide and thus becomes considerable in the visible region [42].

As the photorefractive effect leads to certain limits in the application of guided-wave devices, especially of those designed for operation in the visible and near-infrared regions of the spectrum, different attempts have been undertaken to eliminate or, at least, to reduce the effect. Though certain advances have been achieved by special thermal treatment (thermal fixing), by MgO-doping and by using PE instead of TI waveguides, this problem remains to be of current interest.

## 4.2 Pyroelectric effects

Thermal stability of  $\text{LiNbO}_3$  devices is limited by the high pyroelectric effect of this material. Rather large instabilities have been found for Mach-Zehnder modulators in Z-cut  $\text{LiNbO}_3$ , when the temperature was changed by a few degrees. However, both Z-cut directional couplers and X-cut interferometers show good thermal stability [43].

### 4.3 DC drift phenomena

Electrical DC bias drift effects have been associated also with the buffer layer ( $\text{SiO}_2$  or  $\text{Al}_2\text{O}_3$ ) which separates the TI waveguides in  $\text{LiNbO}_3$  from the metal electrodes. Current leakage through this buffer layer is the most common source of drift. Certain improvement has been achieved by separation of the buffer layer in the gap region of a directional coupler switch [44] and by the annealing of the oxide layer in order to reduce its conductivity.

When a transparent conductive buffer layer (indium tin oxide – ITO) is used, the stability of Mach-Zehnder modulators has been found to be better than 0.3% in 8 h [45].

Recently it has been demonstrated that sputter-etching of more than 20 nm of the  $\text{LiNbO}_3$  substrate surface after waveguide fabrication results in a remarkable suppression of the drift [46]. Obviously, a surface layer with electric conductivity and dielectric parameters different from the bulk material is removed during this process. Though this problem is still under investigation, several applicable approaches for its solution have been presented already.

## 5. EXPERIMENTAL RESULTS

To illustrate the properties of integrated-optical components described above, some samples realized in authors' laboratories are presented.

### 5.1 Mach-Zehnder interferometric modulators

Two types of MZ modulators (see Fig. 2a) were realized, both by TI technology.

In the first case an arrangement with two Y-branchings was used as shown in Fig. 10. For the single-mode operation at the  $1.15 \mu\text{m}$  wavelength, the 65 nm thick and

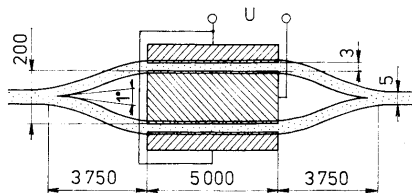
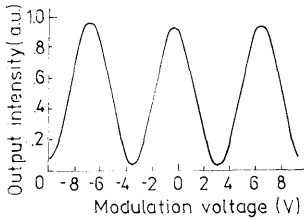


Fig. 10. The arrangement of the fabricated Mach-Zehnder modulator.

$5 \mu\text{m}$  wide titanium pattern was diffused into the X-cut Y-propagating  $\text{LiNbO}_3$  substrate at  $1000^\circ\text{C}$  for 8 h in a Pt box. Then, the Al electrode pattern was delineated by a standard lift-off technique. Although the electrode gap of  $3 \mu\text{m}$  is smaller than the waveguide width, no dielectric buffer layer was used. For endfire coupling the

sample was cut and polished at the ends. The excess loss of the waveguiding structure is about 3 dB compared to a straight non-overlaid waveguide. The loss is evenly distributed among the two Y-branchings with bends (twice 1 dB) and the electrode absorption (1 dB). The low-frequency modulation characteristic is shown in Fig. 11. The modulation voltage of 3.4 V agrees very well with the calculated value of 3.3 V. The extinction ratio of 22.5 dB is limited by slight asymmetry of the Y-branchings. No significant voltage drift was observed within the voltage interval of  $\pm 10$  V.



**Fig. 11.** The measured modulation characteristics of the MZ modulator depicted in Fig. 10.

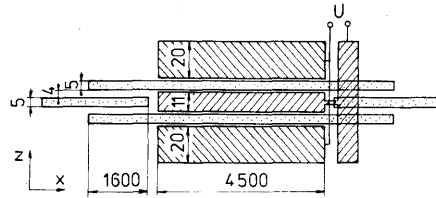


**Fig. 12.** The alternative arrangement of the fabricated MZ-modulator using input and output gate couplers.

The other type [47] uses a pair of optical gate couplers to divide the input light equally into the two arms and recombine it at the output (see Fig. 12). The gate coupler is based on three coupled waveguides. The component is fabricated by TI into a Y-cut  $\text{LiNbO}_3$  at 1000 °C for 6 hours using the platinum-box technology described above. The initial titanium strip width and thickness were 5  $\mu\text{m}$  and 50 nm, respectively, which yielded low-loss waveguides (1 dB/cm or less) suitable for single TE mode propagation in X-direction at  $\lambda = 0.85 \mu\text{m}$ . The waveguides and electrode structures were made photolithographically using electron-beam written masks. The Ni/Au-electrodes of 1.5  $\mu\text{m}$  thickness were fabricated by an electroplating process. The crystal end faces were cut and polished to facilitate endfire coupling. As results the modulation voltage 3.1 V and optical throughput loss 2.4 dB have been measured. The calculated bandwidth is 4.4 GHz.

## 5.2 Directional-coupler switch

The directional-coupler switch with two sections of  $\Delta\beta$ -reversal electrodes shown in Fig. 13 was designed and fabricated [48] by the diffusion of 60 nm Ti into Z-cut

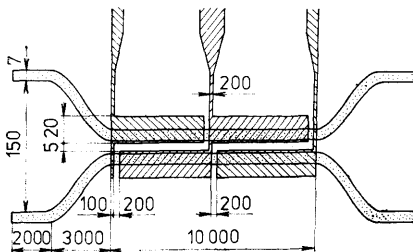


**Fig. 13.** The arrangement of the fabricated directional coupler switch with two sections of electrodes for  $\Delta\beta$  reversal.

LiNbO<sub>3</sub> at 1000 °C for 8 h. The Al electrode patterns was separated from the waveguides by 200 nm buffer layer of Al<sub>2</sub>O<sub>3</sub>. The 1 dB excess loss due to waveguide bends was measured. Low-frequency switching characteristics are shown in Fig. 14.

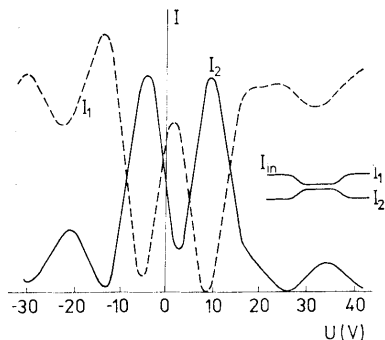


Fig. 14. The measured switching characteristics of the directional coupler switch.

The switching voltage of 8.2 V and the worst-case crosstalk of -17 dB were measured. The calculated voltage was 7.4 V. The RC-limited bandwidth was calculated to be 0.7 GHz. Measurements made up to 300 MHz did not show any significant decrease of the modulation depth.

### 5.3 X-switches

Two types of X-switches as in Fig. 5b were designed and fabricated by the two technologies described above.

In both cases X-cut LiNbO<sub>3</sub> substrates oriented for Y-propagation were used. The outline of initial evaporated Ti stripes and of chromium mask for PE as well as of the electrode structure is shown in Fig. 15a, b. Technological parameters corresponding to the operating wavelength  $\lambda = 0.85 \mu\text{m}$  were as follow:

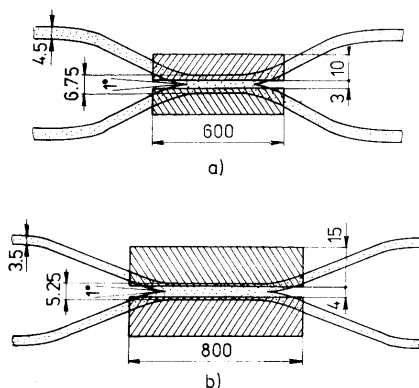
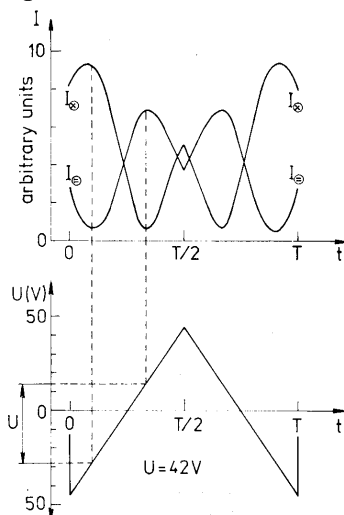


Fig. 15. The arrangement of the fabricated X-switches: a) simple X-switch prepared by TI, b) BOA switch prepared by PE.

- TI: titanium layer thickness 60 nm, Pt-box, diffusion temperature 1050 °C and time 5 h.
- PE: benzoic acid with 1 mol. % lithium benzoate, exchange time 5 h at the temperature 180 °C, subsequent annealing 1 hour at the temperature of 340 °C in oxygen atmosphere.

The thickness of aluminium electrodes was 140 nm; in order to avoid short-circuiting the electrodes by surface currents and to screen off environmental influences the structure is covered by a protective resist.

The measured losses were 1 dB for TI switch and 2 dB for PE switch without coupling loss.



**Fig. 16.** The measured modulation characteristics of the fabricated X-switch depicted in Fig. 15a.

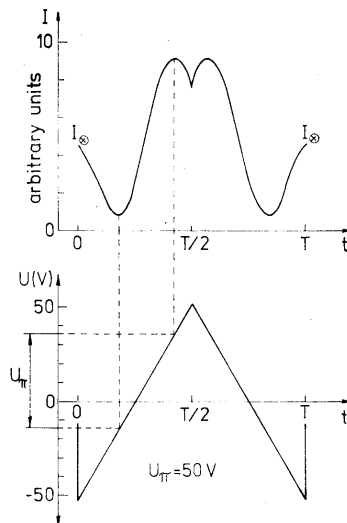


**Fig. 17.** The measured modulation characteristics of the fabricated BOA switch depicted in Fig. 15b.

To suppress the influence of possible drifts, the dynamic measurement was performed using a saw-tooth voltage at the frequency 33 Hz with the peak-to-peak value 100 V. From the characteristics obtained (Figs. 16, 17) the switching voltages  $U_{\pi} = 42$  V and 50 V follow for TI and PE switches, respectively. These values agree rather well with those calculated theoretically. Crosstalk of  $-25$  dB and on-off ratio of about 25 dB have been measured. Further optimization of waveguide parameters and better adjusting of electrode pattern will result in lower loss.

## 6. CONCLUSIONS

Waveguide  $\text{LiNbO}_3$  devices seem to become mature. Above we have described the operation of single-mode modulators and switches designed and fabricated in our laboratories. However, lots of questions are to be answered in order to have

reliably working practical devices. Deeper physical understanding of titanium diffusion and proton exchange is required to improve the reproductibility of the fabrication process. Considerably more extensive study of all stability problems is needed, too. A lot of refining techniques to improve the overall performance of the devices may be applied, e.g., the tailoring of mode field distribution at the waveguide end for the lowest fiber-to-chip coupling loss as well as for the lowest bend loss and/or for the lowest power requirements at the electrooptically active device sections, suppression of unwanted Fresnel reflections at the LiNbO<sub>3</sub>-fiber interface by anti-reflection coating or angled coupling, application of phase- or velocity-matching techniques to increase the modulation or switching speed etc., and other potential techniques newly developed. Series of X and/or BOA switches have to be designed and tested to verify the theoretical predictions and to compare the performance with that of the directional-coupler switches.

Thus, LiNbO<sub>3</sub> electrooptic waveguide devices represent a category of modern optoelectronic components with a potential of further development and improvements, and with promising applications in high-speed optical communication systems (fast external modulators, time-division multi- and demultiplexers), interferometric optical fiber sensors (phase modulators for Mach-Zehnder, Michelson and Sagnac fiber interferometers) and coherent communications (polarizing devices and phase modulators). We are working towards some of these goals.

(Received June 22, 1989.)

#### REFERENCES

- 
- [1] S. E. Miller: Integrated optics: an introduction. *Bell Syst. Tech. J.* **48** (1969), 2059—2069.
  - [2] R. V. Schmidt and I. P. Kaminow: Metal-diffused optical waveguides in LiNbO<sub>3</sub>. *Appl. Phys. Lett.* **25** (1974), 458—460.
  - [3] J. L. Jackel, C. E. Rice and J. J. Veselka: Proton exchange for high-index waveguides in LiNbO<sub>3</sub>. *Appl. Phys. Lett.* **41** (1982), 607—608.
  - [4] W. E. Martin: A new waveguide switch/modulator. *Appl. Phys. Lett.* **26** (1975), 562—564.
  - [5] M. Papuchon et al.: Electrically switched optical directional coupler: COBRA. *Appl. Phys. Lett.* **27** (1975), 289—291.
  - [6] H. Kogelnik and R. V. Schmidt: Switched directional couplers with alternating  $\Delta\beta$ . *IEEE J. Quant. Electron.* *QE-12* (1976), 396—402.
  - [7] A. Neyer: Electrooptic X-switch using single-mode Ti:LiNbO<sub>3</sub> channel waveguides. *Electron. Lett.* **19** (1983), 553—554.
  - [8] M. Papuchon, A. M. Roy and D. B. Ostrowsky: Electrically active optical bifurcation: BOA. *Appl. Phys. Lett.* **31** (1977), 266—267.
  - [9] L. Thylén, A. Djupsjöbacka, M. Janson and W. Döldinen: Integrated optic device for high speed databusses. *Electron. Lett.* **21** (1985), 491—493.
  - [10] W. A. Stallard, A. R. Beaumont and R. C. Booth: Integrated optic devices for coherent transmission. *J. Lightwave Technol.* *LT-4* (1986), 852—857.
  - [11] P. Granstrand et al: Strictly nonblocking  $8 \times 8$  integrated optical switch matrix. *Electron. Lett.* **22** (1986), 816—818.
  - [12] A. Neyer, W. Mevenkamp and B. Kretzschmann: Nonblocking  $4 \times 4$  switch array with 16 switches in Ti:LiNbO<sub>3</sub>. *Proc. IGWO, 1986, pap. WAA2.*

- [13] J. E. Watson, M. Milbrodt and T. C. Rice: A polarization independent  $1 \times 16$  guided wave optical switch integrated on lithium niobate. *J. Lightwave Technol.* *LT-4* (1986), 1717–1721.
- [14] H. F. Taylor: Application of guided wave optics in signal processing and sensing. *Proc. IEEE* *75* (1987), 1524–1535.
- [15] J. Čtyroký, M. Hofman, J. Janta and J. Schröfel: 3-D analysis of  $\text{LiNbO}_3$ :Ti channel waveguides and directional couplers. *IEEE J. Quantum Electron.* *QE-20* (1984), 400–409.
- [16] P. V. Schmidt: Integrated optics switches and modulators. In: *Integrated Optics* (S. Martellucci and A. N. Chichester, eds.), Plenum Press, New York 1983, pp. 181–210.
- [17] J. Čtyroký: Voltage-length product of  $X$  and  $Z$ -cut  $\text{Ti:LiNbO}_3$  directional coupler and BOA switches: a comparison. *J. Opt. Commun.* *4* (1986), 139–143.
- [18] T. K. Findakly and F. J. Leonberger: On the crosstalk of reversed  $\Delta\beta$  directional coupler switches. *J. Lightwave Technol.* *6* (1988), 36–40.
- [19] J. Čtyroký: Guided-wave electro-optic  $X$ -type switches: symmetry, switching characteristics and cross-talk. *J. Modern Optics* *35* (1988), 1007–1015.
- [20] K. Goel and W. S. C. Chang: Effect of asymmetry on extinction coefficient of crossing channel  $\text{LiNbO}_3$  waveguide switches. *Proc. SPIE 835: Integrated optical circuit engineering V*, August 17–20, 1987, pp. 118–125.
- [21] P. Granstrand, L. Thylén and B. Stolz: Polarization independent  $\text{LiNbO}_3$  switch with reduced fabrication tolerances employing  $\Delta\beta$  and  $\kappa$  modulation. *Tech. Digest. Integrated and guided wave optics, Top. Meeting, March 28–30, 1988. Santa Fé*, pp. 244–247.
- [22] R. C. Alferness: Polarization-independent optical directional coupler switch using the weighted coupling. *Appl. Phys. Lett.* *35* (1979), 748–750.
- [23] M. Izutsu, Y. Yamane and T. Sueta: Broad-band travelling-wave modulator using a  $\text{LiNbO}_3$  optical waveguide. *IEEE J. Quantum Electron.* *QE-13* (1977), 287–290.
- [24] R. A. Becker: Travelling-wave electrooptic modulator with maximum bandwidth-length product. *Appl. Phys. Lett.* *45* (1984), 1168–1170.
- [25] L. Thylén and A. Djupsjöbacka: Bandpass response travelling-wave modulator with a transit-time difference compensation schema. *J. Lightwave Technol.* *LT-3* (1985), 47–51.
- [26] K. Miura, M. Minakata and S. Kawakami: Perfect velocity matching of a travelling-wave integrated-optic modulator with high efficiency. *CLEO '88, April 1988*, pp. 288–289.
- [27] J. L. Jackel, V. Ramaswamy and S. P. Lyman: Elimination of out-diffused surface guiding in Ti-diffused  $\text{LiNbO}_3$ . *Appl. Phys. Lett.* *38* (1981), 509–511.
- [28] A. Rasch, M. Rottschalk and W. Karthe: Suppression of out-diffusion in  $\text{Ti:LiNbO}_3$ . *J. Opt. Commun.* *6* (1985), 14–17.
- [29] J. Neyer and T. Pohlmann: Fabrication of low-loss titanium-diffused  $\text{LiNbO}_3$  waveguides using a closed platinum crucible. *Electron. Lett.* *23* (1987), 1187–1188.
- [30] M. Minakata, K. Kumagai and S. Kawakami: Lattice constant changes and electro-optic effects in proton-exchanged  $\text{LiNbO}_3$  optical waveguides. *Appl. Phys. Lett.* *49* (1986), 992–994.
- [31] T. Suhara, S. Fujiwara and H. Nishihara: Proton-exchanged Fresnel lenses in  $\text{Ti:LiNbO}_3$  waveguides. *Appl. Opt.* *25* (1986), 3379–3383.
- [32] J. J. Veselka and G. A. Bogert: Low-loss TM-pass polarizer fabricated by proton exchange for  $Z$ -cut  $\text{Ti:LiNbO}_3$  waveguides. *Electron. Lett.* *23* (1987), 29–31.
- [33] M. Rottschalk, A. Rasch and W. Karthe: Electrooptic behaviour of proton-exchange  $\text{LiNbO}_3$  optical waveguides. *J. Opt. Commun.* *9* (1988), 19–23.
- [34] P. C. Suchoski, M. M. Abu el leil, T. K. Findakly and F. J. Leonberger: In: *Integrated and Guided-Wave Optics Topical Meeting IGWO-88, Santa Fé 1988*, p. 88.
- [35] A. M. Glass: The photorefractive effect. *Optical Engng.* *17* (1978), 470–480.
- [36] R. A. Becker and R. C. Williamson: Photorefractive effects in  $\text{LiNbO}_3$  channel waveguides: Model and experimental verification. *Appl. Phys. Lett.* *47* (1985), 1024–1026.

- [37] A. R. Beaumont, C. G. Atkins and R. C. Booth: Optically induced drift effects in lithium niobate electro-optic waveguide devices operating at a wavelength of 1.51  $\mu\text{m}$ . *Electron. Lett.* 22 (1986), 1260—1261.
- [38] C. T. Müller and E. Garmire: Photorefractive effect in  $\text{LiNbO}_3$  directional couplers. *Appl. Opt.* 23 (1984), 4348—4351.
- [39] G. T. Harvey, G. Astfalk, A. Y. Feldblum and B. Kassahun: The photorefractive effect in titanium indiffused lithium niobate optical directional couplers at 1.3  $\mu\text{m}$ . *IEEE J. Quantum Electr.* QE-22 (1986), 939—946.
- [40] R. L. Holman, J. Busch, M. Parmanter and P. J. Cressman: Lithium Niobate waveguides and their susceptibility to optical damage. *Ferroelectrics* 50 (1983), 171—177.
- [41] E. M. Zolotov, P. G. Kazanskii and V. A. Chernykh: Fotoindutsirovanoe preobrazovanie polarizatsii v kanalnykh Ti-LiNbO<sub>3</sub> volnovodakh. *Pisma v Zh. Tekh. Fiz.* 7 (1981), 924—926.
- [42] R. V. Schmidt, P. S. Gross and A. M. Glass: Optically induced crosstalk in  $\text{LiNbO}_3$  waveguide switches. *J. Appl. Phys.* 51 (1980), 90—93.
- [43] C. H. Bulmer, W. K. Burns and S. C. Hiser: Pyroelectric effects in  $\text{LiNbO}_3$  channel-waveguide devices. *Appl. Phys. Lett.* 48 (1986), 1036—1038.
- [44] S. Yamada and M. Minakata: DC drift phenomena in  $\text{LiNbO}_3$  optical waveguide devices. *Jap. J. Appl. Phys.* 20 (1981), 733—737.
- [45] C. M. Gee, G. D. Thurmond, H. Blauvelt and H. W. Yen: Minimizing dc drift in  $\text{LiNbO}_3$  waveguide devices. *Appl. Phys. Lett.* 47 (1985), 211—213.
- [46] T. Fujiwara, S. Sato, H. Mori and Y. Fujii: Suppression of crosstalk drift in Ti:LiNbO<sub>3</sub> waveguide switches. *J. Lightwave Technol.* LT-6 (1988), 909—915.
- [47] A. Rasch: Untersuchungen an ausgewählten wellenleitenden Ti:LiNbO<sub>3</sub>-Strukturen für einen integriert-optischen Mach-Zehnder-Interferometer-Modulator. Ph. D. Thesis, FS University, Jena 1988.
- [48] J. Čtyroký, J. Janta and J. Schröfel: Electrooptic guided-waveguide switch in  $\text{LiNbO}_3$  (in Czech). *Slaboproudý obzor* 48 (1987), 116—122.
- [49] K. Komatsu, S. Yamazaki, M. Kando and Y. Ohta: Low-loss broad-band  $\text{LiNbO}_3$  guided-wave phase modulators using titanium magnesium double diffusion method. *J. Lightwave Technol.* LT-5 (1987), 1239—1245.

*Ing. Jiří Čtyroký, CSc., Ing. Jiří Janta, CSc., Ústav radiotechniky a elektroniky ČSAV (Institute of Radio Engineering and Electronics — Czechoslovak Academy of Sciences), Lumumbova 1, 182 51 Praha 8. Czechoslovakia.*

*Dr. Rolf Göring, Prof. Dr. Wolfgang Karthe, Dr. Andreas Rasch, Dr. Mathias Rottschalk, Friedrich-Schiller-Universität, Sektion Physik (Friedrich Schiller University, Section of Physics), Max-Wien-Platz 1, Jena 6900. German Democratic Republic.*

*Ing. Josef Schröfel, CSc., Tesla-VÚST (Tesla - Research Institute of Communications), Novodvorská 994, 142 21 Praha 4. Czechoslovakia.*